Dependence on CO adsorption of the shapes of multifaceted gold nanoparticles: A density functional theory

Georgios D. Barmparis*
Department of Materials Science and Technology, University of Crete, 71003 Heraklion, Crete, Greece, and Institute of Electronic Structure & Laser, Foundation for Research and Technology–Hellas, 71110 Heraklion, Crete, Greece

Ioannis N. Remediakis†
Department of Materials Science and Technology, University of Crete, 71003 Heraklion, Crete, Greece
(Received 27 November 2011; revised manuscript received 11 May 2012; published 30 August 2012)

We present a computational study for the environment-dependent equilibrium shape of gold nanoparticles. By linking extensive quantum-mechanical calculations, based on density functional theory (DFT), to Wulff constructions, we predict the equilibrium shapes of clean and CO-covered gold nanoparticles. We construct atomistic models of nanoparticles with diameters up to several tenths of a nanometer, inaccessible by direct atomistic simulations. Au nanoparticles smaller than 16.3 nm in diameter have truncated octahedral shape, exposing only (111) and (100) faces. Larger nanoparticles also expose higher-index faces, mostly (332). We study the adsorption of CO on several different Au surfaces, and we use the results to obtain the interface energy between Au and CO at low pressure and temperature. These results are then used to obtain the equilibrium shape of Au nanoparticles in CO gas. In agreement with experimental data, Au nanoparticles in CO are found to be more spherical and more reactive compared to Au nanoparticles in noninteracting environments.

DOI: 10.1103/PhysRevB.86.085457 PACS number(s): 81.10.Aj, 68.43.Fg, 82.65.+r

I. INTRODUCTION

Bulk gold is the noblest of all metals,[1] as demonstrated by delicate gold jewels manufactured several millennia ago which are found intact in excavations. On the other hand, catalysts that include oxide-supported gold nanoparticles were found to efficiently oxidize CO at room temperature;[2–4] Au is by far the best such catalyst.[5,6] Among the key factors that determine the efficiency of Au catalysts is the shape of Au nanoparticles, in particular the 5- and 6-fold coordinated atoms at its corners.[7–9]

The shape of Au nanoparticles has a key role in every aspect of their functionality, from sensing[10] and biolabeling applications[11] to plasmonics[12] and photonics.[13] In optoelectronics, quantum leaps between electronic states transform light into electricity and vice versa. The probability of such a transition depends on the density of states and the dipole matrix elements according to Fermi's golden rule. For a given size, both wave functions and energies depend critically on the nanoparticle shape. For example, the lowest excitation energy for a cubic nanoparticle is 10% higher than that of a spherical nanoparticle of the same volume.[14]

Gold nanoparticles are often found in their equilibrium shape. At the thermodynamic limit, this is a polyhedron enclosed by faces of various (hkl) crystal orientations such that the total surface energy,

$$\sum_{hkl} A_{hkl}\gamma_{hkl}, \tag{1}$$

is minimum. A_{hkl} is the total area of faces parallel to the (hkl) plane of the crystal and γ_{hkl} is the energy required to create a surface of unit area that is parallel to the (hkl) plane of the crystal and is the analog of the surface tension of liquids. Here, for reasons of simplicity, we will use the term surface tension as a synonym for surface energy per unit area.

In order to predict equilibrium shape, one needs calculations of surface tensions for many different (hkl) surfaces. Several such calculations exist in the literature for Au, some based on empirical potentials,[15] others limited to Miller indexes of 0 and 1,[16,17] and still others using quantum mechanics for low-index faces and empirical models for higher indexes.[18] An accurate and systematic calculation of all high-index Au surfaces is lacking.

Nanoparticle shape is often found to change upon exposure to some interacting environment. For Au nanoparticles, changes to shapes of higher sphericity upon exposure to CO have been observed both experimentally[19] and theoretically.[20] The interface tension of a metal in equilibrium with a gas is found to depend on the surface tension, the adsorption energy, and the coverage of adsorbates. In order to predict the equilibrium shape in an interacting environment using the Wulff construction method, it is necessary to have a systematic calculation of adsorption energies for all relevant (hkl) surfaces.

The Wulff construction has been used to predict equilibrium shapes in a variety of systems. Wulff polyhedra are often employed in observations and models for nanomaterials including Cu catalysts[21,22] or semiconductors.[23] In the past decade, Wulff shapes employing surface tensions from first-principles calculations were used for the successful prediction of the shape of nanoparticles, including interactions with their environment.[17,24–29] In the context of ammonia-synthesis catalysis, an *ab initio* determination of a nanoparticle shape was used as a first step in the creation of a virtual nanocatalyst.[30–32] In that work, the Wulff polyhedron was filled with atoms in order to create a realistic nanoparticle. The advantage of this method was that it allowed for detailed analysis of the atomic positions, making it possible to calculate structural quantities such as the number of active sites. This virtual nanocatalyst was used in other similar reactions, such as ammonia decomposition.[32] Here, we expand this methodology by including all possible (hkl) orientations. Moreover, we

take into account changes in shape that may be induced by interactions between the nanoparticle and its environment. We apply our method to supported gold nanoparticles, a system of high technological importance.

The paper is organized as follows: in Sec. II, we briefly review Wulff's theory regarding the equilibrium shape. In Sec. III, we present a systematic calculation of the surface tension for every Au(hkl) surface with Miller indexes up to 4. In Sec. IV, we use these surface tensions to create atomistic models for Au nanoparticles of sizes up to 100 nm, and we analyze their structural properties, such as the concentration of active sites. In Sec. V, we present the adsorption of CO on gold surfaces with Miller indexes up to 3 and discuss trends on adsorption energies. In Sec. VI, we provide a simple formula that relates the interface tension to the surface tension and adsorption energy and use the results from CO adsorption to calculate the change in equilibrium shape of Au particles upon exposure to CO gas. We summarize our results in Sec. VII.

II. THE WULFF CONSTRUCTION

The concept of "equilibrium shape" was postulated by Gibbs in the late 19th century. Under thermodynamic equilibrium, a given quantity of matter will attain a shape that minimizes the total surface energy of the system. More than a century ago, mineralogist G. Wulff proposed that the shape that minimizes Eq. (1) is such that the distance of each face from the center is proportional to the surface tension of the respective (hkl) surface:[33]

$$d_{hkl} \sim \gamma_{hkl}. \tag{2}$$

One begins the Wulff construction by drawing up a plane [for example, (111)] at a distance d_{111} from the origin followed by planes parallel to (hkl) at distances $d_{hkl} = d_{111}\gamma_{hkl}/\gamma_{111}$. The equilibrium shape will be the polyhedron enclosed by these planes, having thus the following properties:

(1) The shape depends on ratios between surface tensions, and not their absolute values.

(2) (hkl) planes with high surface tension (usually high-indexed ones) will be drawn at greater distances and are therefore less likely to appear in the equilibrium shape.

(3) Being steeper, high-index faces are usually hidden behind low-index ones, and they tend to occupy smaller areas in the equilibrium shape even if γ_{hkl} is low.

(4) The extra energy associated with the formation of edges between two surfaces is not taken into account.

(5) The Wulff polyhedron belongs to the same point group as the crystal structure of the material.

In addition to Wulff construction, there exist other methods for the study of nanoparticles. Advances in computers allow for the direct simulation of nanoparticles of large sizes using empirical potentials, as done for example by McKenna.[20] In that work, a large number of different shapes are tested to find the lowest-energy one. The Wulff construction is complementary to that method. Here, we use Wulff construction coupled to first-principles calculations of surface tensions, in order to study large nanoparticles inaccessible by atomistic simulations.

III. SURFACE TENSION OF GOLD SURFACES

We begin by calculating the surface tension, γ_{hkl}, of Au by simulations of periodic (hkl) slabs using density functional theory (DFT). We use the open-source Dacapo/ASE suite (https://wiki.fysik.dtu.dk). We use a plane-wave basis with 340 eV cutoff. The core electrons are treated with Vanderbilt nonlocal ultrasoft pseudopotentials.[34] The Brillouin zone of the (111)-(1 × 1) surface is modeled by a (10 × 10 × 1) Monkhorst-Pack grid of $\vec{k}$ points; the number of $\vec{k}$ points in other surfaces is calculated in proportionality to the (111) cell. We use the generalized gradient approximation (GGA) Perdew-Wang exchange-correlation functional (PW91) for the clean surfaces and the revised Perdew-Burke-Ernzerhof functional (RPBE) for the surfaces covered with CO since this one gives better adsorption energies.[35] For each set of calculations, we use the theoretical lattice constant, which is found to be 4.18 Å for PW91 and 4.22 Å for RPBE, both of which are very close to the experimental value of 4.08 Å. There is a general trend to slightly overestimate the lattice constant of noble metals using GGA.[36] We model all (hkl) surfaces of fcc Au with indexes up to 4. No ($4kl$) surfaces are observed in the Wulff constructions we find; for this reason we do not consider ($5kl$) surfaces in this work. Atoms in the top two layers from each side are allowed to relax, while subsequent slabs are separated by 12 Å of vacuum. Slab thickness is chosen independently for each (hkl) slab until the surface tension converges within 0.01 J/m^2.

The surface energy per unit area or surface tension, γ_{hkl}, is derived from a simulation of bulk gold followed by a simulation of a slab with faces parallel to (hkl):

$$E_{\text{slab}} = N E_{\text{bulk}} + 2A\gamma_{hkl}, \tag{3}$$

TABLE I. Ratios of surface tensions of Au in comparison to other calculations. For Ref. 18, we list values derived from an empirical model followed by values from *ab initio* calculations (in parentheses).

	This work	Ref. 15	Ref. 18	Ref. 17	Ref. 16
$\gamma_{100}/\gamma_{111}$	1.23	1.11	1.15 (1.18)	1.20	1.27
$\gamma_{110}/\gamma_{111}$	1.29	1.24	1.23 (1.27)	1.27	1.33
$\gamma_{210}/\gamma_{111}$	1.33	1.31	1.29 (1.34)		
$\gamma_{211}/\gamma_{111}$	1.17	1.19	1.18 (1.20)		
$\gamma_{221}/\gamma_{111}$	1.14	1.16	1.15		
$\gamma_{310}/\gamma_{111}$	1.31	1.28	1.28		
$\gamma_{311}/\gamma_{111}$	1.26	1.24	1.22 (1.24)		
$\gamma_{320}/\gamma_{111}$	1.36	1.30	1.28		
$\gamma_{321}/\gamma_{111}$	1.25	1.26	1.23		
$\gamma_{322}/\gamma_{111}$	1.11	1.13	1.12		
$\gamma_{331}/\gamma_{111}$	1.18	1.21	1.19 (1.22)		
$\gamma_{332}/\gamma_{111}$	1.07	1.11	1.11		
$\gamma_{410}/\gamma_{111}$	1.32	1.25	1.26		
$\gamma_{411}/\gamma_{111}$	1.27	1.23	1.22		
$\gamma_{421}/\gamma_{111}$	1.32	1.29	1.26		
$\gamma_{430}/\gamma_{111}$	1.34	1.29	1.27		
$\gamma_{431}/\gamma_{111}$	1.27	1.27	1.25		
$\gamma_{432}/\gamma_{111}$	1.19	1.20	1.18		
$\gamma_{433}/\gamma_{111}$	1.09	1.09	1.09		
$\gamma_{441}/\gamma_{111}$	1.22	1.22	1.21		
$\gamma_{443}/\gamma_{111}$	1.06	1.09	1.08		

where N is the number of atoms in the slab, E_{slab} is the total energy of the slab, E_{bulk} is the energy per atom in bulk Au, and A is the area parallel to (hkl).

The results are summarized in Table I. Interestingly, the ratio of surface energies of different cells is very close to the ratio of the areal density of cleaved bonds.[18] This is another example of the unique chemistry of Au:[1] Au atoms have a closed d shell and have the least preference for directional bonds in the entire periodic table. The calculated absolute value for γ_{111} is 0.69 J/m^2, which is very close to the values of 0.64 J/m^2 reported by Wen and Zhang[15] and 0.72 J/m^2 reported by Shi and Stampfl[17] who used a method similar to the one used here. Moreover, our value is within the same order of magnitude as the values reported by state-of-the-art relativistic all-electron calculations.[16,18] The nanoparticle shape depends only on ratios between surface energies. As shown in Table I, our results for the ratios between surface tensions agree with more detailed calculations within 5% or less.

IV. Au NANOPARTICLES IN A NONINTERACTING ENVIRONMENT

The Wulff construction for Au is shown in Fig. 1(c). It contains 144 vertices and 86 faces of 5 different kinds: (111), (332), (100), (211), and (322) in order of total area.

To construct atomistic models for nanoparticles, we start from a large fcc simulation cell. We consider two initial configurations, one where a Au atom resides at the origin and another where the octahedral hollow site is at the origin. The first configuration yields nanoparticles with odd number of (111) layers, while the second one yields nanoparticles with even number of (111) layers. We focus on (111) as this face has the lowest surface tension. We begin by choosing the number of (111) layers. This determines the distance of the (111) plane from the center of the nanoparticle, d_{111}, and, consequently, the nanoparticle size. For other faces, we use Eq. (2), with the calculated values of γ_{hkl}, and cut the crystal at the correct distances d_{hkl}. This leads to a faceted nanoparticle. Using Cartesian coordinates for the atoms, we calculate the equations of planes for the nanoparticle faces, and we make sure they are consistent with the (hkl) planes predicted by Wulff's theorem. We consider about 30 000 different nanoparticles with diameters ranging from 1 to more than 100 nm.

As we are interested in relatively large Au nanoparticles, we limit our study to nanoparticles where Au atoms far from the surfaces are in the ideal fcc lattice. This is observed in simulations of large clusters,[38] although small gold clusters may have structures very different from fcc.[39]

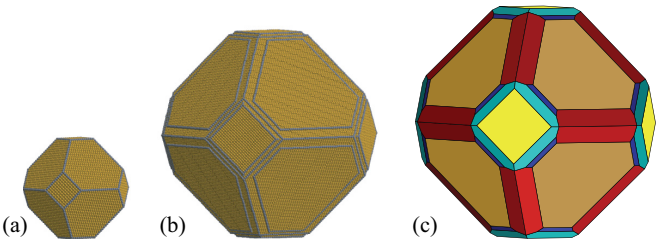

FIG. 1. (Color online) Typical calculated Au nanoparticles for various sizes, d: (a) $d = 12.1$ nm (b) $d = 27.2$ nm, and (c) $d \to \infty$. In (a) and (b), step and kink atoms are shown in darker color. In (c), different colors correspond to different kinds of surfaces. (c) was created using Wulffman software.[37]

At small sizes, some faces might not be large enough to accommodate a single atom, let alone a unit cell of this surface. Very small nanoparticles expose only (111) and (100) faces. Interestingly, the Wulff construction seems to agree with several minimum-energy structures of large Au clusters found by direct DFT simulations by Barnard and Curtiss.[40] In particular, we find that Au_{19}, Au_{44}, and Au_{85} nanoparticles have octahedron shape, Au_{38}, Au_{79}, and Au_{140} ones truncated octahedron shape, and Au_{55} and Au_{116} cuboctahedron shape, which are identical to the corresponding lowest-energy structures of Barnard and Curtis.[40] Gold clusters that do not contain an integer number of (100) and (111) layers are not accessible by the present method. X-ray diffraction experiments[38] have confirmed the shape of Au_{79} and Au_{140} found here and by Barnard and Curtis;[40] moreover, our work agrees with these experimental findings for larger clusters such as Au_{225} and Au_{459}. We find the latter to contain thirteen (100) layers, the smallest of which contains nine atoms, in excellent agreement with the results of Cleveland *et al.*[38]

This agreement between Wulff construction, experiment, and atomistic simulations at such small sizes is surprising and should again be attributed to the unique chemistry of Au: Au-Au bonds have extremely low directionality, as manifested by the very low shear modulus of bulk gold. It is therefore very unlikely that Au atoms will prefer to lower their coordination numbers in order to obtain a more favorable bond angle geometry, as would be that case for clusters of elements with unpaired electrons, such as Si or Ni.

For sizes 2 nm and higher, the shape resembles a truncated octahedron consisting mainly of (111) and (100) faces, with their edges decorated by several (hkl) faces with indexes up to 3. Nanoparticles with diameter up to 16.3 nm have a truncated octahedron shape with only (111) and (100) faces, as shown in Fig. 1(a). As the nanoparticle grows in size, different (hkl) orientations start to appear [see Fig. 1(b)]. The thermodynamic limit, shown in Fig. 1(c), is reached at diameters of the order of 100 nm.

Au nanoparticles adsorbed on C nanotubes are often found in such truncated octahedral shapes. Bittencourt and co-workers[41,42] present various transition electron microscopy (TEM) images of nanotube-supported Au nanoparticles that are very similar to the ones presented here. For example, comparing our nanoparticle at about 5 nm diameter to Fig. 1 of Ref. 41, we find the same shape: the angle between long edges is 105° (115° in experiment) while the angle between long and short edges is 125° (130° in experiment). For Au nanoparticles supported on TiO_2, Sivaramakrishnan *et al.*[43] provide an atomistic image of nanoparticles that best fit TEM experiments and the Wulff theorem. For a nanoparticle of about 5 nm in diameter, they find a truncated octahedral shape, where the hexagonal faces have edges that are eight and five atoms long. For a similar size, we find the same shape with a similar aspect ratio (eight to six for our case). Given the errors introduced from processing TEM images, the agreement between theory and experiment is good.

Geometrical features of typical nanoparticles are shown in Table II. The area of the nanoparticles is calculated

TABLE II. Characteristic data for typical nanoparticles shown in Fig. 1. Shape (a) is typical for particles up to $d = 16.3$ nm in diameter, shape (b) is typical for larger particles, and (c) presents fitted values from over a hundred different particles. N_v, N_e, and N_f are the total number of atoms at vertices, edges, and faces of the nanoparticle, respectively; N_t is the total number of atoms. N_{act} is the number of active sites and (hkl) are the appearing surfaces in the shape with the percentage of the total area they occupy.

Shape	d (nm)	N_v	N_e	N_f	N_t	Area (nm^2)	Volume (nm^3)	Sphericity (%)	N_{act} (μmol/g)	Faces
(a)	12.12	24	444	5208	42925	438	730	89.6	55	(111), (100) (86%), (14%)
(b)	27.17	96	2832	25998	473550	2172	8439	92.3	31	(111), (332), (100), (211) (60%), (17%), (12%), (11%)
(c)	$0.31N^{0.34}$	144	$N^{0.60}$	$3N^{0.68}$	N	$0.3N^{0.67}$	0.02N	92.9	$5077/N^{0.40}$	(111),(332),(100),(211),(322)

analytically using the coordinates of vertices; their volume is obtained by numerical integration. The sphericity[44] of a nanoparticle equals $\pi^{1/3}(6V)^{2/3}/A$, where V is the volume and A the area; characteristic values are 81% for a cube, 85% for an octahedron, and 100% for a sphere. Since in Au-based catalysis step-edge sites are usually responsible for the chemical activity, we also provide the number of active sites per gram of material, N_{act}, assuming that only step-edge atoms are active. By fitting over 100 particles of different diameters, we provide scaling relations of various properties with total number of atoms, in accordance with atom-counting models for nanoparticles.[45,46]

V. CO ADSORPTION ON Au SURFACES

In this section, we investigate the adsorption of CO molecules on Au(hkl) with $(h,k,l \leqslant 3)$ surfaces. The adsorption energy of CO on gold surfaces is needed in order to calculate the interface tension of a CO-covered gold surface.

In general, the adsorption energy of a molecule X on a surface, E_{ads}, is defined as the excess energy per molecule of the system compared to an isolated Au surface and isolated encapsulating material and is given by

$$E_{\text{slab}+X} = E_{\text{slab}} + N_{\text{ads}} E_X + N_{\text{ads}} E_{\text{ads}}, \tag{4}$$

where $E_{\text{slab}+X}$ is the total energy of the slab + X system, E_X is the total energy per molecule of X, and N_{ads} is the number of bonds between the slab and X.

To calculate the minimum adsorption energy of CO on every Au(hkl) surface with $h,k,l \leqslant 3$, we perform total energy calculations of CO-covered gold slabs, using the same methodology we used to obtain surface tensions. The only difference is that we use the RPBE exchange-correlation functional since this one gives better adsorption energies for CO.[35] The first two layers and the CO molecule are free to relax. As we are interested in very low CO coverage, neighboring CO molecules maintain a distance of more than 4.2 Å in all cases.

We begin by calculating the adsorption energy for several different adsorption sites of the planar (100), (110), and (111) surfaces. We use this calculation as a guide for the investigation of the preferred adsorption site for CO on other surfaces. For Au(100) and Au(110) we found that bridge and on-top adsorption sites are the most stable ones and that hollow sites are highly unfavorable. For Au(111), CO was found to adsorb weakly with little preference for a specific adsorption site. These results agree with most theoretical and experimental works from the literature (see Ref. 47 and references therein). For this reason, we limited the investigation for the adsorption sites only to bridge and on-top sites for stepped and kinked surfaces. We start with an 8-Å-thick slab and consider several different initial bridge- and on-top-adsorption configurations. For the two best among them, we increase the slab thickness until the ratio of adsorption energy over area per adsorbate converges to 10 mJ/m^2. In Fig. 2, we present the minimum adsorption energy of CO as a function of the slab thickness for two typical surfaces. For planar surfaces, the adsorption energy has a weak dependence on slab thickness, as was found by Mavrikakis *et al.*[48] In contrast, stepped and kinked surfaces show large variations of adsorption energy as the slab thickness increases, as shown in Fig. 2 for (310). For this reason, large simulation cells are necessary in order to calculate the adsorption energy for high-index surfaces.

The results for adsorption energies, bond lengths, and angles are summarized in Table III. The microfacet notation[49] provides a concise way to describe stepped surfaces, as it shows the type and width of the terraces and the orientation of the steps. In the following, we compare our findings to other experimental and theoretical works.

For Au(110), we find $E_{\text{ads}} = -0.36$ eV, which is in excellent agreement with the experimental value of -0.35 eV.[50] For Au(111) we find a very weak adsorption with $E_{\text{ads}} = -0.02$ eV for the on-top site, which is close to the value of -0.04 eV calculated by Hammer *et al.*[51] The choice of

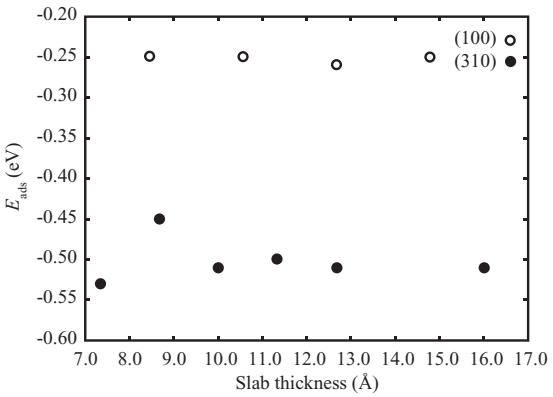

FIG. 2. The adsorption energy of CO on Au(100) and Au(310) as a function of the slab thickness.

TABLE III. Adsorption energy of CO on gold surfaces at low coverage. The adsorption geometry is shown in parentheses; b stands for bridge-site adsorption and t stands for on-top adsorption. Also shown are the Au-C bond length, $d_{\text{Au-C}}$, the height between the carbon atom and the surface, $dz_{\text{Au-C}}$, the C-O bond length, $d_{\text{C-O}}$, and the average angle between Au-C and C-O bonds, $\theta_{\text{Au-C-O}}$.

Surface	Mictofacet notation	E_{ads} (eV)	$d_{\text{Au-C}}$ (Å)	$dz_{\text{Au-C}}$ (Å)	$d_{\text{C-O}}$ (Å)	$\theta_{\text{Au-C-O}}$ (degrees)
(100)	(100)	−0.25(b)	2.14	1.44	1.18	132
(110)	(110)	−0.36(b)	2.14	1.48	1.18	134
(111)	(111)	−0.02(t)	2.00	1.99	1.16	180
(210)	2(110)×(100)	−0.49(t)	2.00	1.99	1.16	174
(211)	3(111)×(100)	−0.34(b)	2.14	1.45	1.18	133
(221)	4(111)×(111)	−0.35(t)	2.02	2.01	1.16	162
(310)	3(100)×(110)	−0.51(t)	1.99	1.98	1.17	169
(311)	2(111)×(100)	−0.32(b)	2.14	1.45	1.18	133
(320)	3(110)×(100)	−0.48(t)	1.99	1.99	1.16	178
(321)	(321)	−0.50(t)	2.00	1.99	1.16	168
(322)	5(111)×(100)	−0.34(t)	2.03	2.02	1.16	161
(331)	3(111)×(111)	−0.34(t)	2.01	2.01	1.16	166
(332)	6(111)×(111)	−0.35(t)	2.03	2.02	1.16	159

exchange-correlation potential is important, as for instance PW91 generally overestimates CO-Au binding.[35,47] For example, for (111) we find an adsorption energy of −0.30 eV using PW91, identical to the value reported by Mavrikakis *et al.*[48] Although adsorption energies change upon changing the exchange-correlation functional, their differences are less sensitive. For the various stepped surfaces that contain (111) terraces, we find adsorption energies between 0.30 and 0.33 eV lower than the adsorption energy for planar (111), within the range of 0.24 to 0.36 eV found in Refs. 48 and 47. For stepped surfaces that contain (110) or (100) terraces and for the kinked Au(321), we find adsorption energies 0.46 to 0.49 eV lower than that for Au(111), which is very close to the value of 0.43 eV found in Refs. 52 and 47. For Au(310), the angle $\theta_{\text{Au-C-O}}$ equals 169.2°, which is very close to 173.1° reported in Ref. 47.

The Au-C bond length, $d_{\text{Au-C}}$, depends only on the adsorption site and has a very weak dependence to the structure of each particular surface. It is close to 2.00 Å for on-top adsorption and 2.14 Å for bridge adsorption. The same holds for the height difference between C-O, $dz_{\text{Au-C}}$. This is the projection of the bond on the (hkl) direction. We find on average 1.46 Å for bridge and 2.00 Å for on-top adsorption, in agreement with 1.5 and 2 Å, respectively, found in Ref. 53.

For on-top adsorption, $dz_{\text{Au-C}}$ is almost equal to $d_{\text{Au-C}}$, showing that CO is almost perpendicular to the surface. In contrast, $dz_{\text{Au-C}}$ is much smaller than $d_{\text{Au-C}}$ for bridge-site adsorption. The values presented in Table III correspond to tilt angles that are smaller than 5° for on-top adsorption whereas they can be up to 47° for bridge adsorption. This is also evident from the angle between Au-C-O, which is close to 180° for on-top adsorption and drops to about 135° for bridge adsorption.

The C-O bond length is between 1.16 and 1.18 Å, slightly longer than that for the gas-phase molecule, which we calculate at 1.15 Å. Other DFT simulations produce values that range from 1.14 to 1.20 Å.[47,52–54] CO adsorbed on bridge sites forms two Au-C bonds and is therefore a little longer than CO adsorbed on top sites, which forms only one Au-C bond.

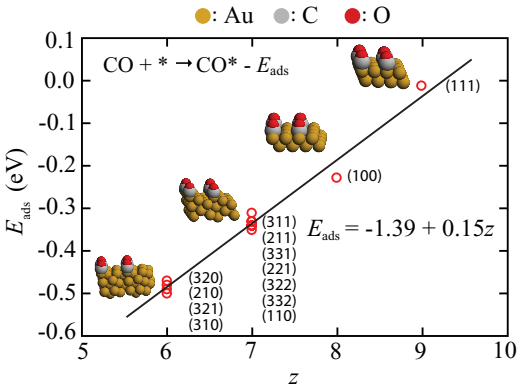

FIG. 3. (Color online) Adsorption energy of CO on Au(hkl) as a function of the Au coordination number, z, and its linear fit. Some characteristic adsorption geometries are shown.

In almost every case, CO binds to the lowest-coordinated Au atoms, in agreement with experimental observations.[55] Simulations for low-index Au surfaces and small clusters have revealed that CO adsorption energy is well described by a linear function of z, where z is the average coordination number of Au atoms that bind to CO.[7–9,56] In Fig. 3 we plot E_{ads} versus z and verify that the linear fit is also valid for high-index stepped and kinked surfaces. To save computational time, we use this linear fit to obtain adsorption energies for the nine $(4kl)$ surfaces.

VI. Au NANOPARTICLES IN AN INTERACTING ENVIRONMENT

The equilibrium shape of nanoparticles that interact with their environment can be found by means of a Wulff construction based on interface tensions, $\gamma_{hkl}^{\text{int}}$, between Au and its environment instead of surface tensions, γ_{hkl}. It turns out that the two are related by the simple formula

$$\gamma_{hkl}^{\text{int}} = \gamma_{hkl} + \theta \frac{E_{\text{ads}}}{A_{\text{at}}}, \tag{5}$$

where $\theta = N_{\text{ads}}/N_{\text{surface}}$ is the coverage (number of adsorbates, N_{ads}, over number of surface atoms, N_{surface}), $A_{\text{at}} = A/N_{\text{surface}}$ is the total surface area, A, over the total number of surface atoms, N_{surface}, and E_{ads} is the adsorption energy. Equation (5) includes implicitly the effects of adsorbate-adsorbate interactions, as both the adsorption energy and the equilibrium coverage depend on such interactions.

To prove this equation, we use the definitions of $\gamma_{hkl}^{\text{int}}$,

$$E_{\text{slab}+X} = N E_{\text{bulk}} + N_{\text{ads}} E_X + 2A\gamma_{hkl}^{\text{int}}, \tag{6}$$

in conjunction with the definition of E_{ads} in Eq. (4). Substituting into Eqs. (6) and (4) and using Eq. (3) yields Eq. (5).

For a typical system ($\theta = 0.1$, $E_{\text{ads}} = -0.5$ eV), the second term in Eq. (5) is about 0.1 J/m^2, or 10% of γ_{hkl}. The change in ratios between various γ_{hkl} will be of the order of 1%, resulting in very small changes in the equilibrium shape. This explains the similarity of nanoparticle shapes observed in a wide variety of environments: our simulations nicely match

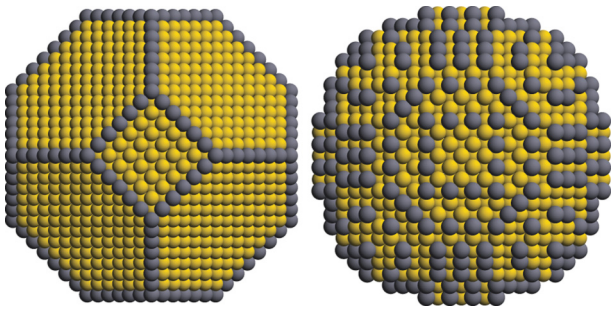

FIG. 4. (Color online) Left: Model of a typical Au nanoparticle ($d = 5.4$ nm, ∼5000 atoms) in a weakly interacting environment (sphericity = 91%, 200 μmol of active sites per gram) Right: The same size nanoparticle in equilibrium with low-pressure CO gas (sphericity = 98%, 400 μmol of active sites per gram). Step and kink atoms are shown in darker color.

experimental observations, not only for Au clusters[38] but also for Au particles on C nanotubes,[41,42] on TiO_2,[43] and on CeO_2.[4] On the other hand, shape can change dramatically for very small nanoparticles where bonding on faces might be very different from bonding on a large surface[57,58] or when small molecules with high adsorption energy, such as CO, are adsorbed.

We use calculated adsorption energies from Sec. V together with Eq. (5) and obtain the equilibrium shape of Au nanoparticles at low CO coverage. A typical nanoparticle is shown in Fig. 4. For rough surfaces, γ_{hkl} will be relatively high, but at the same time E_{ads} will be quite low; this results in a compensation effect for the two terms in Eq. (5). As the different $\gamma^{\text{int}}_{hkl}$ are close to each other, the shape has higher sphericity. For the nanoparticle shown in Fig. 4, sphericity increases from 91% to 98%. This change of Au nanoparticles toward rounder shapes upon exposure to reactive environments has also been observed in experiments. Ueda *et al.*[19] observed in TEM experiments that the shape of supported gold nanoparticles changed upon exposure to CO gas toward an almost semispherical shape and the crystal habit was sometimes observed with facets on the surface. Also, Uchiyama *et al.*[4] used *in situ* environmental transmission electron microscopy (ETEM) and observed that faceted gold nanoparticles, dominated by (111) and (100) faces, became rounded when exposed to reactive gases.

The reactivity of Au nanoparticles is likely to arise from step-edge atoms, as pointed out by Lemire *et al.*[59] With this assumption, we find that exposure of the nanoparticle to CO gas makes it much more reactive. This effect has been already observed in simulations of small Au clusters.[8,20,60] The same happens at larger sizes, although the effect is more pronounced for smaller nanoparticles. If one assumes that all step-edge atoms are active, the active-site density doubles, increasing from about 200 to about 400 μmol/g for the nanoparticle shown in Fig. 4.

Gold nanoparticles are usually supported on oxides, such as MgO or rutile TiO_2. The interaction between the nanoparticle and the supporting material will also affect its shape. The epitaxial growth will introduce strain in the nanoparticle.[23] More importantly, the values of γ_{hkl} for the faces attached to the supporting material will be very different. A qualitative picture of this interaction has been presented by Lopez *et al.*[61]

VII. SUMMARY

We have constructed and characterized gold nanoparticles in thermodynamic equilibrium, including interactions with their environment. We first studied all low-index Au(hkl) surfaces, both clean and with CO molecules adsorbed on them. Approximate formulas found for low-index surfaces hold also for high-index stepped and kinked surfaces: the surface tension is roughly proportional to the density of cleaved metal bonds, while the CO adsorption energy is a linear function of the Au coordination number. Using an atomistic version of the Wulff construction, we generate Cartesian positions of atoms in large nanoparticles that are of interest to catalysis but are inaccessible by direct atomistic simulations. The simulated nanoparticles match experimental results, including the similarity of shapes in weakly interacting systems as well as the change toward more spherical shapes upon exposure to CO gas.

ACKNOWLEDGMENTS

This work was supported by COST action MP0901 (NanoTP) and by the Research Committee, University of Crete. The authors acknowledge support from and inspiring discussions with S. Farantos.

*barmparis@materials.uoc.gr
†remed@materials.uoc.gr; Group Web Page: http://theory.materials.uoc.gr

[1] B. Hammer and J. K. Nørskov, Nature (London) **376**, 238 (1995).
[2] M. Haruta, N. Yamada, T. Kobayashi, and S. Iijima, J. Catal. **115**, 301 (1989).
[3] M. Valden, X. Lai, and D. W. Goodman, Science **281**, 1647 (1998).
[4] T. Uchiyama, H. Yoshida, Y. Kuwauchi, S. Ichikawa, S. Shimada, M. Haruta, and S. Takeda, Angew. Chem. Int. Ed. **50**, 10157 (2011).
[5] B. Hvolbæk, T. V. W. Janssens, B. S. Clausen, H. Falsig, C. H. Christensen, and J. K. Nørskov, Nano Today **2**, 14 (2007).
[6] H. Falsig, B. Hvolbaek, I. S. Kristensen, T. Jiang, T. Bligaard, C. H. Christensen, and J. K. Nørskov, Angew. Chem. Int. Ed. **47**, 4835 (2008).
[7] N. Lopez and J. K. Nørskov, J. Am. Chem. Soc. **124**, 11262 (2002).
[8] I. N. Remediakis, N. Lopez, and J. K. Nørskov, Angew. Chem. Int. Ed. **44**, 1824 (2005).
[9] I. N. Remediakis, N. Lopez, and J. K. Nørskov, Appl. Catal. A **291**, 13 (2005).
[10] Y. Kim, R. Johnson, and J. Hupp, Nano Lett. **1**, 165 (2001).
[11] E. Boisselier and D. Astruc, Chem. Soc. Rev. **38**, 1759 (2009).
[12] S. Lal, S. Link, and N. J. Halas, Nat. Photonics **1**, 641 (2007).
[13] Y. Lu, Y. Yin, Z. Li, and Y. Xia, Nano Lett. **2**, 785 (2002).
[14] For a cube of edge a, $\Delta E = 3\frac{\hbar^2\pi^2}{2ma^2} = 29.61\frac{\hbar^2}{2ma^2}$; for a sphere of radius r and volume a^3, $\Delta E = \frac{\hbar^2(\chi_{11}^2-\chi_{10}^2)}{2mr^2} = 26.82\frac{\hbar^2}{2ma^2}$, where χ_{11} and χ_{10} are the first two roots of the spherical Bessel function $j_1(x)$.

[15]Y.-N. Wen and J.-M. Zhang, Solid State Commun. **144**, 163 (2007).
[16]L. Vitos, A. V. Ruban, H. L. Skriver, and J. Kollr, Surf. Sci. **411**, 186 (1998).
[17]H. Shi and C. Stampfl, Phys. Rev. B **77**, 094127 (2008).
[18]I. Galanakis, G. Bihlmayer, V. Bellini, N. Papanikolaou, R. Zeller, S. Blügel, and P. H. Dederichs, Europhys. Lett. **58**, 751 (2002).
[19]K. Ueda, T. Kawasaki, H. Hasegawa, T. Tanji, and M. Ichihashi, Surf. Interface Anal. **40**, 1725 (2008).
[20]K. P. McKenna, Phys. Chem. Chem. Phys. **11**, 4145 (2009).
[21]B. S. Clausen, J. Schiøtz, L. Gråbæk, C. V. Ovesen, K. W. Jacobsen, J. K. Nørskov, and H. Topsøe, Top. Catal. **1**, 367 (1994).
[22]P. L. Hansen, J. B. Wagner, S. Helveg, J. R. Rostrup-Nielsen, B. S. Clausen, and H. Topsøe, Science **295**, 2053 (2002).
[23]P. Müller and R. Kern, Surf. Sci. **457**, 229 (2000).
[24]A. Barnard and P. Zapol, J. Chem. Phys. **121**, 4276 (2004).
[25]A. S. Barnard and L. A. Curtiss, Nano Lett. **5**, 1261 (2005).
[26]G. Hadjisavvas, I. N. Remediakis, and P. C. Kelires, Phys. Rev. B **74**, 165419 (2006).
[27]G. Kopidakis, I. N. Remediakis, M. G. Fyta, and P. C. Kelires, Diam. Relat. Mater. **16**, 1875 (2007).
[28]F. Mittendorfer, N. Seriani, O. Dubay, and G. Kresse, Phys. Rev. B **76**, 233413 (2007).
[29]A. Soon, L. Wong, B. Delley, and C. Stampfl, Phys. Rev. B **77**, 125423 (2008).
[30]K. Honkala, A. Hellman, I. N. Remediakis, A. Logadottir, A. Carlsson, S. Dahl, C. Christensen, and J. K. Nørskov, Science **307**, 558 (2005).
[31]A. Hellman, K. Honkala, I. N. Remediakis, A. Logadottir, A. Carlsson, S. Dahl, C. H. Christensen, and J. K. Nørskov, Surf. Sci. **600**, 4264 (2006).
[32]A. Hellman, K. Honkala, I. N. Remediakis, A. Logadottir, A. Carlsson, S. Dahl, C. H. Christensen, and J. K. Nørskov, Surf. Sci. **603**, 1731 (2009).
[33]C. Herring, Phys. Rev. **82**, 87 (1951).
[34]D. Vanderbilt, Phys. Rev. B **41**, 7892 (1990).
[35]B. Hammer, L. B. Hansen, and J. K. Nørskov, Phys. Rev. B **59**, 7413 (1999).
[36]M. Fuchs, M. Bockstedte, E. Pehlke, and M. Scheffler, Phys. Rev. B **57**, 2134 (1998).
[37]A. R. Roosen, R. P. McCormack, and W. C. Carter, Comput. Mater. Sci. **11**, 16 (1998).
[38]C. L. Cleveland, U. Landman, M. N. Shafigullin, P. W. Stephens, and R. L. Whetten, Z. Phys. D **40**, 503 (1997).
[39]F. Baletto and R. Ferrando, Rev. Mod. Phys. **77**, 371 (2005).
[40]A. S. Barnard and L. A. Curtiss, Chem. Phys. Chem. **7**, 1544 (2006).
[41]C. Bittencourt, A. Felten, B. Douhard, J.-F. Colomer, G. V. Tendeloo, W. Drube, J. Ghijsen, and J.-J. Pireaux, Surf. Sci. **601**, 2800 (2007).
[42]M. Quintana, X. Ke, G. V. Tendeloo, M. Meneghetti, C. Bittencourt, and M. Prato, ACS Nano **4**, 6105 (2010).
[43]S. Sivaramakrishnan, J. Wen, M. E. Scarpelli, B. J. Pierce, and J.-M. Zuo, Phys. Rev. B **82**, 195421 (2010).
[44]H. A. Wadell, J. Geol. **3**, 250 (1935).
[45]N. Lopez, T. Janssens, B. Clausen, Y. Xu, M. Mavrikakis, T. Bligaard, and J. K. Nørskov, J. Catal. **223**, 232 (2004).
[46]N. V. Galanis, I. N. Remediakis, and G. Kopidakis, Phys. Status Solidi C **7**, 1372 (2010).
[47]A. Hussain, D. Curulla Ferré, J. Gracia, B. E. Nieuwenhuys, and J. W. Niemantsverdriet, Surf. Sci. **603**, 2734 (2009).
[48]M. Mavrikakis, P. Stoltze, and J. Nørskov, Catal. Lett. **64**, 101 (2000).
[49]M. A. Van Hove and G. A. Somorjai, Surf. Sci. **92**, 489 (1980).
[50]D. A. Outka and R. J. Madix, Surf. Sci. **179**, 351 (1987).
[51]B. Hammer, Y. Morikawa, and J. K. Nørskov, Phys. Rev. Lett. **76**, 2141 (1996).
[52]D. Loffreda and P. Sautet, J. Phys. Chem. B **109**, 9596 (2005).
[53]F. Mehmood, A. Kara, T. S. Rahman, and C. R. Henry, Phys. Rev. B **79**, 075422 (2009).
[54]M. G. A. Eichler and J. Hafner, J. Phys.: Condens. Matter **16**, 1141 (2004).
[55]I. Nakamura, A. Takahashi, and T. Fujitani, Catal. Lett. **129**, 400 (2009).
[56]G. Mpourmpakis, A. N. Andriotis, and D. G. Vlachos, Nano Lett. **10**, 1041 (2010).
[57]M. Walter, J. Akola, O. Lopez-Acevedo, P. D. Jadzinsky, G. Calero, C. J. Ackerson, R. L. Whetten, H. Groenbeck, and H. Häkkinen, Proc. Natl. Acad. Sci. USA **105**, 9157 (2008).
[58]W. D. Luedtke and U. Landman, J. Phys. Chem. B **102**, 6566 (1998).
[59]C. Lemire, R. Meyer, S. Shaikhutdinov, and H.-J. Freund, Angew. Chem. Int. Ed. **43**, 118 (2004).
[60]K. P. McKenna and A. L. Shluger, J. Phys. Chem. C **111**, 18848 (2007).
[61]N. Lopez, J. Nørskov, T. Janssens, A. Carlsson, A. Puig-Molina, B. Clausen, and J.-D. Grunwaldt, J. Catal. **225**, 86 (2004).